Nuclear Engineering and Design 416 (2024) 112803

Contents lists available at ScienceDirect

Nuclear Engineering and Design

journal homepage: www.elsevier.com/locate/nucengdes

Study of the impact of hydrides on the fracture toughness of Zr-2.5Nb alloy

Remigijus Janulionis *, Gintautas Dundulis

Lithuanian Energy Institute, Breslaujos str. 3, Kaunas LT-44403, Lithuania

ARTICLE INFO

Keywords:
Finite element method
Fracture toughness
Hydrogen absorption
Zr-2.5Nb alloy
Fuel channel

ABSTRACT

Hydrogen absorption and hydride formation in zirconium (Zr) alloys is a well-known issue and has been extensively studied in the past. Hydrogen has an impact not only on the strength but also on the fracture toughness of Zr alloys. As various Zr alloys are used for manufacturing the core components of nuclear reactors, such as nuclear fuel claddings, fuel channels, fuel assemblies, fixtures, and etc., their structural integrity has a great impact on the safety and reliability of the whole nuclear power plant. Furthermore, the hydrogen absorption ageing mechanism retains its significance not just during reactor operation but also throughout decommissioning and storage of spent nuclear fuel, especially when sufficient levels of absorbed hydrogen concentrations are reached, potentially leading to a delayed hydride cracking mechanism. Assessing the impact of hydrogen absorption on the strength of zirconium alloys typically involves time-consuming, costly, and sample-intensive experimental studies. Consequently, there is a demand for alternative research approaches. This article introduces the methodology to evaluate the fracture toughness of the Zr-2.5Nb alloy with varying hydrogen concentrations.

1. Introduction

Zirconium alloys are used for the production of pressure tubes, fuel cladding, fuel assemblies, and fasteners in nuclear power plants (NPP). Zr-2.5Nb alloy is used in the production of pressure tubes and fuel channels (FC) of Russian high-power channel-type reactor (RBMK), Canadian pressurized heavy-water reactor (CANDU), Karachi nuclear power plant (KANUPP), Japan nuclear reactor (FUGEN) and other types of reactors (Ishizuka et al., 2003; Almenas et al., 1998; Cheadle et al., 1996). Zry-2, Zry-4, or Zr-1Nb alloys are usually used in the production of nuclear fuel claddings (IAEA, 2006). Fuel claddings are important structural elements of the active reactor zone and, like fuel channels, are subject to high operational reliability and durability requirements. Zirconium alloys function under rigorous conditions, boasting a low thermal neutron absorption cross section, excellent corrosion resistance, and favourable physical as well as mechanical properties. However, like other structural materials, zirconium alloys do age during operation, i.e., their properties change over time. The ageing mechanisms that affect the Zr alloys and the effect that accompany them are presented in Table 1 (IAEA, 1999).

The exterior surface of the nuclear fuel cladding remains in continuous contact with the coolant (water). The high temperature and the water environment are the conditions that cause corrosion. During the corrosion of Zr alloys, as a side effect, hydrogen is produced, which is later absorbed by fuel channels and fuel claddings. In the α phase of zirconium, the solubility limit of hydrogen is extremely low, measuring less than 1 ppm at room temperature, around 70–80 ppm at 300 °C, and around 200 ppm at 400 °C (Kearns, 1967; Motta et al., 2019). When the hydrogen concentration exceeds the solubility limit, hydrogen and zirconium form a brittle hydride in the zirconium matrix (Suman et al., 2015) resulting in degradation of the physical and mechanical properties of the alloy. At low temperatures, the brittleness increases, and at reactor operating temperatures, FC or fuel claddings can begin to crack due to the delayed hydride cracking (DHC). It is a consequence of the hydrogen absorption ageing mechanism. DHC is a crack growth mechanism met in materials with hydrides, where brittle hydrides migrate to the higher stress region, usually to the tip of the initial flaw, and under load a small portion of the material is braking (cracking). As a result, a small growth of crack is obtained (IAEA, 2004). DHC has been identified in the pressure tubes and fuel channels of many reactors and has been the main reason for their damage (IAEA, 2006; Ivanova, 2002). There are also known cases of DHC in CANDU pressure tubes in Canada (Cheadle et al., 1987) and damage to the FC of RBMK reactors (Platonov et al., 1988) caused by the DHC mechanism.

The first time DHC was observed in the pressure tubes of Canadian CANDU reactors. In light-water reactors, the DHC mechanism was discovered only in the late 90s. It was found in high-burnup fuel

* Corresponding author.
E-mail address: Remigijus.janulionis@lei.lt (R. Janulionis).

https://doi.org/10.1016/j.nucengdes.2023.112803
Received 31 August 2023; Received in revised form 20 November 2023; Accepted 26 November 2023
Available online 2 December 2023

Nomenclature

Latin

Δa	Crack extension (mm)
a	Total crack length (mm)
a_1	Fatigue crack length (mm)
B	C(T) specimen' thickness (mm)
E	Modulus of elasticity (MPa)
J_I	J-integral (kN/m)
J_{IC}	Elastic-plastic fracture toughness (kN/m)
J_Q	Conditional Elastic-plastic fracture toughness (kN/m)
K_I	Stress intensity factor (MPa$\sqrt{m}$)
K_{IC}	Critical stress intensity factor (MPa$\sqrt{m}$)
K_Q	Conditional stress intensity factor (MPa$\sqrt{m}$)
$K_I{}^*$	Stress intensity factor at P_{max} (MPa$\sqrt{m}$)
P	Tension force (N)
P_{max}	Maximal tension force, N
P_Q	Conditional tension load (N)
T	Temperature (K)
V	Crack opening displacement (mm)
W	C(T) specimen' width (mm)
Z	Reduction of specimen's cross-sectional area (%)

Greek

ε_f	Failure strain (%)
$\sigma_{0.2}$	Yield strength (MPa)
σ_U	Ultimate strength (MPa)

Acronym

A-T	Axial-tangential plane
C(T)	Compact tension specimen
CANDU	Canadian pressurized heavy-water reactor (Canada Deuterium Uranium)
DHC	Delayed hydride cracking
FC	Fuel channels
FE	Finite element
FEM	Finite element method
FUGEN	Japan nuclear reactor
KANUP	Karachi nuclear power plant
LBB	Leak before brake
NPP	Nuclear power plant
R-A	Radial-axial plane
R-T	Radial-tangential plane
RBMK	Russian high-power channel-type reactor
TMT-2	Thermo-mechanical treatment No. 2
VVER	Russian water-water energetic reactor
Zr	Zirconium

Table 1
Mechanisms of ageing of Zr alloy.

Mechanisms of ageing	Effect
Irradiation hardening and embrittlement	Change of mechanical properties
Static and cyclic metal damage	Growth of defect in material
Hydrogen absorption	General embrittlement
Corrosion	Reduction of wall thickness
Irradiation creep	Change of dimensions

claddings of boiling water reactors.

Recently, the relevance of the DHC mechanism has increased in intermediate spent nuclear fuel storage repositories, since the spent nuclear fuel stored in pools has absorbed sufficient amounts of hydrogen for the DHC mechanism to occur during the operation period (Alvarez Holston and Stjärnsäter, 2017). During the operation of a nuclear reactor, fission gases and other products are released from fuel pallets. Additional amounts of gases increase the pressure inside fuel cladding. Due to the higher inner pressure, the fuel cladding stresses also increase, together with the hydride precipitates, caused by hydrogen absorption ageing mechanism, creates favourable conditions for DHC to occur and for the formation and growth of cracks (Videm et al., 1979). Small flaws formed in the wall of the fuel cladding may increase during spent nuclear fuel storage (Hong et al., 2017) or even grow through the wall of the cladding. The DHC mechanism is also identified as the reason for fuel cladding and fuel channel failure in VVER and RBMK reactors (IAEA, 2004; Ivanova, 2002). However, often the causes of these components remain unexplained or attributed to other factors due to the complicated investigation procedure of highly irradiated materials (Kim, 2008; Grigoriev and Josefsson, 1998).

Numerous scientific articles could be found on the influence of hydrogen absorption on the mechanical properties of zirconium alloys, which proves the importance of the issue. Chakraborty et al. (2015) conducted a study and demonstrated how the properties of pure zirconium change depending on the hydrogen concentration. The zirconium specimen was saturated with very high hydrogen concentrations: from 1 % to 5 %. Research has shown that the strength limit of zirconium decreased up to 30 % with an increase of hydrogen concentration at 5 %. The strains, at which zirconium failed, also decreased while the hydrogen concentration increased, but not as significant as the strength limit: at 5 % hydrogen concentration, the strain decreased by about 10 %.

Silva et al. (2018) conducted research on the Zr-2.5Nb alloy used in CANDU nuclear reactors. The studied material was purchased in plate form and manufactured by ATI Wah Chang (USA). The alloy was heat treated at the factory, i.e., thermal annealing and rapid cooling of the alloy in the β phase was performed. Later, the material was saturated with hydrogen in the laboratory, and tensile tests were performed. Comparing the test results of the initial material and those saturated with hydrogen up to 285 ppm has shown a mild change in the yield and ultimate strength of the alloy. A larger change to the ultimate strength (22 % reduction) was recorded at a hydrogen concentration of 320 ppm. However, results revealed that hydrogen has a greater influence not on the strength but on the plastic strain of the material at its ultimate strength level. At a hydrogen concentration of 285 ppm, the ultimate strain was reduced by 65 % compared to the strain of the material without hydrogen and even up to 81 % at a hydrogen concentration of 320 ppm. Indian scientists Bind et al. (2016), who studied a Zr-2.5Nb alloy pressure tube supplied by the Nuclear Power Corporation of India, obtained similar results. It was found that hydrogen has a small influence on the yield and strength limits, but a significant influence on plastic strain (the plastic strains decrease by 40 % at a hydrogen concentration of 199 ppm). Interestingly, Bind et al. tests also carried out at higher temperatures (up to 300 °C). Plastic strain reduction of similar magnitude was found to occur in the entire temperature range 25 °C $\leq$ T $\leq$ 300 °C. These studies confirm that zirconium and its alloys have lower plastic strain and become more brittle when absorbed hydrogen. Even at higher temperatures, when part of the zirconium hydrides dissolves, the plastic strain is still affected by hydrogen. Brittle materials are less resistant to fracture, and the reduced plastic strain level of the material has a significant impact on the fracture toughness of zirconium alloy.

One of the first studies of the Zry-2 alloy (Yeniscavich et al., 1959) showed that the strength limit of the fuel cladding material up to 500 ppm hydrogen concentration remains constant within the experimental data error interval. However, when the concentration exceeds 500 ppm, the strength limit of Zry-2 starts to decrease significantly. Although the

specimen elongation vs. hydrogen concentration results had scattered in fairly wide limits, a tendency towards elongation reduction is still clearly observable when the hydrogen concentration exceeds 100 ppm.

During the study of Zry-4 mechanical properties dependence on hydrogen concentration (Lin et al., 1979) an interesting change in the ultimate strength limit was recorded. As the hydrogen concentration increased to 400 ppm, the ultimate strength limit of Zry-4 had also increased by approximately 10 %, and after the hydrogen concentration exceeded 400 ppm only then the strength limit began to decrease. When the hydrogen concentration reached 1500 ppm, the strength limit dropped 10 % below the initial value. It is also interesting that a consistent increase in the yield strength of Zry-4 is observed throughout the hydrogen concentration range. Despite the increase in strength and yield strength, the elongation of the specimen was consistently decreasing along with increasing hydrogen concentration. More recent studies of the mechanical properties of Zry-4 were performed in the circumferential direction of the fuel cladding (Kim et al., 2007; Jang and Kim, 2017). Both of the aforementioned studies were performed not only at room temperature, but also at higher temperatures. Kim et al. (Kim et al., 2007), consistent with the previously described studies (Lin et al., 1979), found that the strength limit of Zry-4 increases with increasing hydrogen concentration. And at the hydrogen concentration of 500 ppm, the strength limit begins to decrease. However, such a change is observed only at room temperature. During the tests at higher temperatures (350 °C and 500 °C), no such phenomenon was detected, i. e., a consistent decrease in the strength limit was observed. The studies by Jang and Kim (2017) also investigated the dependence of the properties of the irradiated Zry-4 alloy on hydrogen concentration. Results have revealed an opposite dependency of the strength limit of the irradiated alloy on the hydrogen concentration compared to the nonirradiated one, i.e., the strength limit decreased with increasing hydrogen concentration, and the largest change of 40 % was found at room temperature.

In 2008, experimental studies of the Zr-2.5Nb alloy with thermomechanical treatment No. 2 (TMT-2) fuel channel were conducted (Daunys et al., 2008). During these studies, an increase in yield and strength limits was observed with increasing hydrogen concentration in the alloy. Similarly, as in studies described above, a reduction in plastic strain level was observed in samples saturated with hydrogen. As the hydrogen concentration changed from 0 to 140 ppm, the relative elongation at failure of the specimen decreased by about 13 %.

A summary of the results of mentioned studies is presented in Fig. 1. A comparison of the strength limit dependence of different zirconium alloys on hydrogen concentration shows that in most studies the strength limit of the material increases up to a hydrogen concentration of 400–500 ppm, and when the hydrogen concentration exceeds the limit of 500 ppm, the strength limit starts to decrease.

As previously described, studies showed that hydrogen has influence not only on the yield and ultimate strength limits of zirconium alloys but also on their plastic strain level. The reduced plastic strain of the material has a significant influence on its fracture toughness. Therefore, a number of studies on the critical stress intensity factor and critical J-integral of different zirconium alloys saturated with hydrogen can be found. Kreyns et al. (1996) demonstrated how the critical stress intensity factor of the Zry-4 alloy is affected depending on different levels of hydrogen concentration (up to 560 ppm) and temperature. The research shows that hydrogen has a strong influence on the stress intensity factor of the Zry-4 alloy at room temperature; however, an effect remains even at higher temperatures. However, when the temperature exceeds 250 °C, the influence of hydrogen decreases significantly.

Simpson and Cann (1979) have presented the stress intensity factor of pure zirconium and the Zr-2.5Nb alloy as a function of high hydrogen concentrations. A linear dependence of the stress intensity factor of pure zirconium on the hydrogen concentration was determined, while the change in the stress intensity factor of the Zr-2.5Nb alloy mainly corresponded to a logarithmic function. In all cases, the value of the stress intensity factor decreased as the hydrogen concentration increased. This was observed in experiments at room temperature and 300 °C. The values of the critical stress intensity factor (K_{IC}) of the Zr-2.5Nb alloy determined at room temperature ranged from 18 to 2 MPa$\sqrt{m}$, and at 300 °C from 39 to 2 MPa$\sqrt{m}$. However, it should be noted that Simpson's and Cann's studies were performed at extremely high hydrogen concentrations, when the ratio of hydrogen to zirconium atoms (H/Zr) varied from 0.1 to 1.6.

Daunys et al. (2008) have studied the Zr-2.5Nb alloy used for the production of FC of RBMK type reactors. The research showed that the material remains quite plastic when the hydrogen concentration increases to 140 ppm. Therefore, only conditional values of the stress intensity factor K_Q and K_C* have been determined. The K_Q value decreased by 9 %, i.e., from 33 to 30 MPa$\sqrt{m}$, and K_C* decreased by 25 % (from 60 to 45 MPa$\sqrt{m}$). As the critical stress intensity factor K_{IC} could not be determined, the J-integral, the parameter that defines the plastic fracture, was studied. During the research, the influence of hydrogen was analysed at both room and elevated temperatures. The results showed that the largest change (84 %) of critical J-integral (J_{IC}) was found at room temperature, where J_{IC} decreased from 95 to 15 kN/m. The 18 %

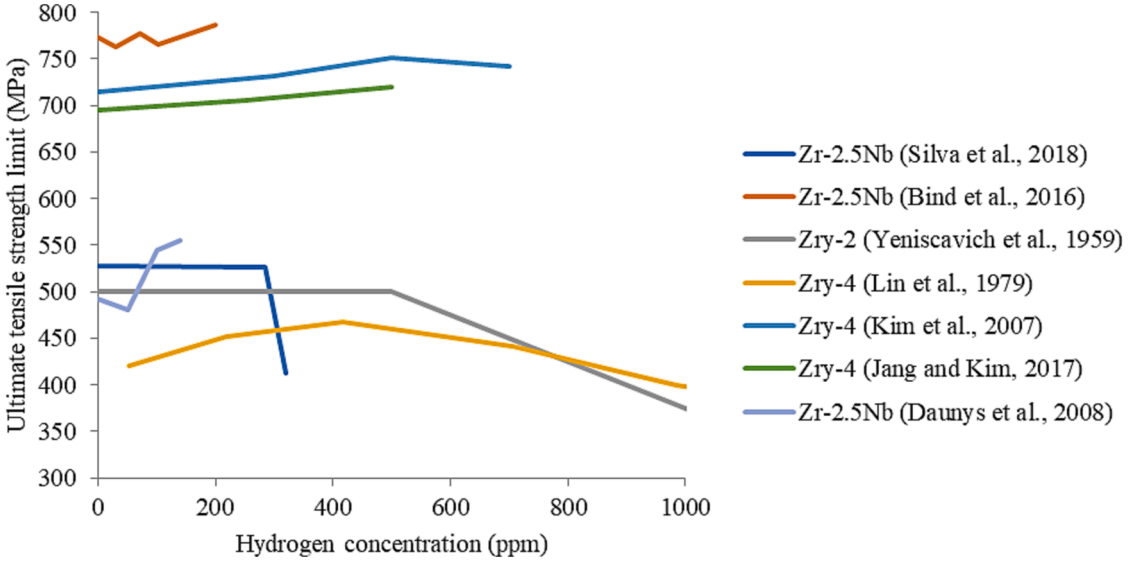

Fig. 1. Ultimate strength limit vs. hydrogen concentration of various zirconium alloys.

decrease in the J_{IC} value (from 66 to 54 kN/m) was observed at 170 °C and a very small change (from 84 to 82 kN/m) at 300 °C.

Hsu (2006) studied the dependency of the J-integral of the Zry-4 alloy on the hydrogen concentration, but determined only J_{max} instead of the J_{IC} value, which is found at the maximum tensile force recorded during the tension of the compact tension (C(T)) specimen (does not comply with the definition of J_{max} in the ASTM E1820-15a (2015) standard). Hsu carried out tests on the fuel cladding material at room temperature and 300 °C with hydrogen concentrations ranging from 0 to 1118 ppm. The determined variation of J_{max} values depending on the hydrogen concentration had a logarithmic dependence. At room temperature, the highest determined J_{max} value of the hydrogen-free Zry-4 alloy reached 122 kN/m and only 19 kN/m at a hydrogen concentration of 1118 ppm. The J_{max} value was also determined at 300° C temperature, where the change was much smaller: from 97 kN/m without hydrogen to 77 kN/m at a hydrogen concentration of 657 ppm. Microstructural analysis of the crack tip of Zry-4 alloys without hydrogen and at 500 ppm hydrogen concentration showed that due to hydrogen embrittlement, the plastic deformation zone is smaller before crack growth, which also reduces the amount of potential energy. Since the J-integral is a parameter that determines the rate of strain energy release, it depends on the change in the amount of potential energy. Hsu also raised the question of the effect of the reduced hydrogen concentration at higher temperatures. The author tends to agree with the opinion of Simpson and Cann (1979) that the influence of hydrogen at temperatures higher than 150 °C is reduced primarily due to increased plastic strain of the zirconium matrix, but not due to improved properties of zirconium hydrides.

Bind et al. (2017) also studies the J-integral of the Zr-2.5Nb alloy used in the manufacture of a pressurised heavy water reactor pressure tube at an Indian nuclear power plant. The research was conducted at room and higher temperatures and at various hydrogen concentrations. The authors of this work came to similar conclusions as the authors of the previously described studies: the influence of hydrogen at room temperature is mainly noticeable from a concentration of 0 to 30 ppm, a further increase of the hydrogen concentration lowers the values of $J_{0.15}$, J_Q, J_{max} and $J_{1.5}$ values, but not significantly; the plot of the J-integral vs. temperature for all samples has the S shape, where the upper shelf is around 200 °C, and only the temperatures of the lower shelf that varies; due to hydrogen embrittlement, the cracks tend to form in the axial direction in the Zr-2.5Nb alloy pressure tube.

Most of the studies found on the properties of zirconium alloys were performed experimentally. However, it is not always possible to conduct experimental studies of the material. First, a sample of the material is needed to make specimens for experimental research. Extracting material from an operational nuclear reactor or a storage facility for spent fuel is a challenging and dangerous task in its own right. Second, the volume of the sampled material must be relatively large, as the specimens for experimental tests must be of standard dimensions. Third, the materials studied in the nuclear industry are often irradiated, so special hot laboratories are needed to handle these materials. All of these factors contribute to the complexity and high price of experimental research. Therefore, alternative material testing and/or prediction methods are needed to evaluate its properties and ensure the safety of nuclear facilities. Research in the literature showed that the finite element method is usually used as an alternative to experimental tests. Varias and Massih (2000) analysed the fracture parameters of the zirconium alloy. A finite element model of the Zr-2.5Nb alloy and two consecutive hydrides at the microlevel was developed. A finite element model was used to determine the threshold stress intensity factor K_{IH} and to develop the analytical model. However, neither analytically nor numerically, the values of the critical fracture toughness parameters were determined. Suman et al. (2017) carried out a numerical simulation of compact specimen tension made of the Zry-4 alloy. The authors using the ABAQUS v6.12 finite element program created a model of a compact specimen with hydrides of different lengths near the tip of the crack. The extended finite element method (XFEM) was used to evaluate the growth of the crack. As a result, the stress intensity factor values and the J-integral values for different hydride and crack dimensions are presented in the article. However, the critical K_{IC} and J_{IC} values of the Zry-4 alloy have not been determined.

Some articles were found in which the numerical determination of critical J-integral J_{IC} of other metals was presented. Jeon et al. (2016) showed a method for numerical determination of the critical integral J-integral of SA508 Gr.3, TP316L and CF8M steels using a complex crack growth model. The results obtained by the proposed method coincide well with the experimental results. However, using this method requires an additional description of the material damage model, which additionally requires the determination of three material constants. For this purpose, the experimental tests of specimens with grooves have to be conducted. Weygand, Mahler, and Aktaa (Weygand and Aktaa, 2009; Mahler and Aktaa, 2014, 2016) also demonstrated a numerical simulation methodology for critical J-integral determination. Numerical simulations were performed for the T91 and EUROFER 97 steels. In their methodology, additional cohesive elements layer has to be modelled; for the description of which, authors use their own developed user subroutine installed in the standard finite element programme ABAQUS.

An extensive literature review shows that the hydrogen absorption ageing mechanism has a significant effect on zirconium alloys, which cannot be neglected and must be evaluated. However, a numerical methodology is needed that allows determining the mechanical and fracture toughness properties of zirconium alloys by only numerical methods, which can later be applied in the analysis of defects detected during nondestructive testing or in leak before brake (LBB) analysis. Nondestructive testing is the type of inspection that allows examining components under operation without causing damage. Whereas LBB is the concept developed in NPPs and shows that in the worst-case scenario, usually for pipes or pressure vessels, if the failure occurs, it starts with the leak for some period of time allowing to take measures to avoid catastrophic failure. In both cases, the mechanical properties of the aged components' materials are needed to make the evaluations. Therefore, this article presents the methodology for the determination of mechanical properties as well as fracture toughness for zirconium alloys with hydrides. Additionally, the article shows the application of the methodology for Zr-2.5 %Nb TMT-2 alloy saturated with hydrogen.

2. Methodology

The main aim of this paper is to present the methodology for the determination of mechanical and fracture toughness properties for zirconium alloy containing hydrides. In this study, the averaged effects of hydrogen to zirconium alloy specimens were evaluated and no local, such as uneven distribution or grouping of Zr hydride, were taken into account, the same as the experiments conducted this study was based on. To achieve the objective, the work is divided into steps that must be carried out according to the algorithm presented in Fig. 2.

As shown in the figure, the mechanical properties of zirconium alloy with hydrides first have to be determined. It has to be evaluated how much the specific hydrogen concentration has changed the elastic modulus, yield and ultimate strength of zirconium alloy compared to those of zirconium alloy without hydrogen. Second, having the mechanical properties of zirconium alloy with hydrides, the critical stress intensity factor K_{IC} has to be determined. If K_{IC} was determined, it means that the brittle fracture toughness of the zirconium alloy with hydrides was found. However, if K_{IC} could not be determined, only a conditional K_Q, that means the material is still too ductile and critical J-integral J_{IC} has to be found, and in this case, it can be stated that ductile fracture toughness of zirconium alloy with hydrides is evaluated.

The review of the scientific literature has revealed that, as an alternative to experiment, the finite element method (FEM) is widely used for numerical determination of fracture toughness. Therefore, in this study, FEM was also selected to assess the fracture toughness and mechanical

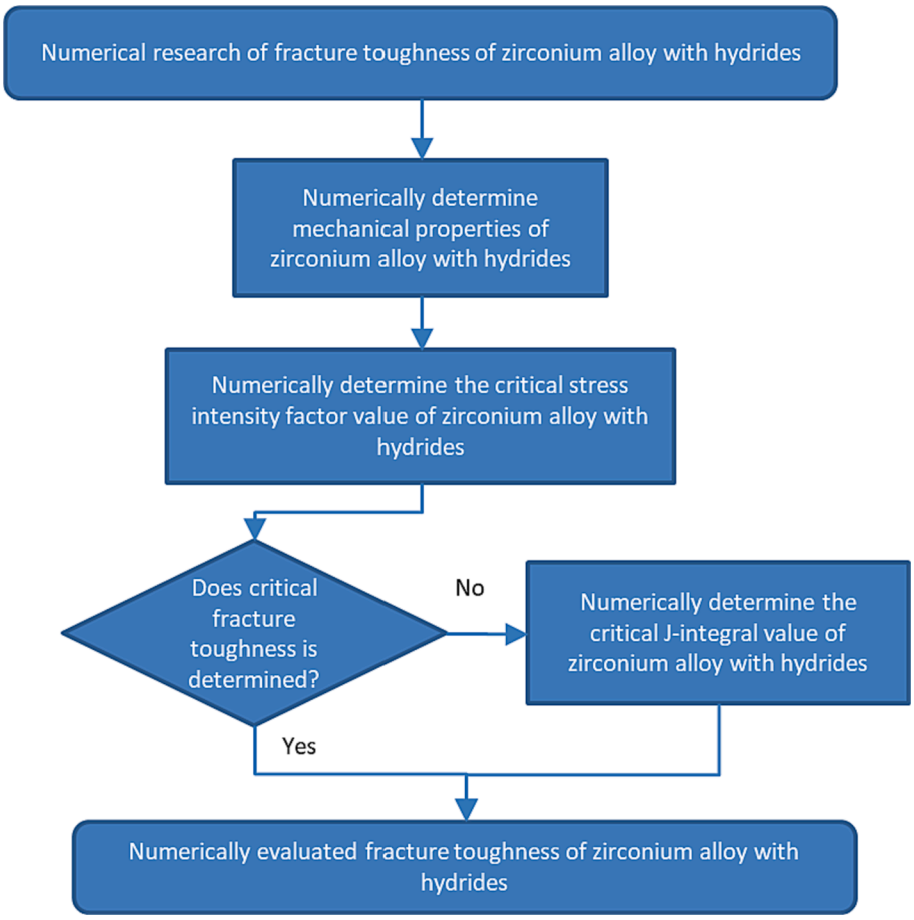

Fig. 2. Algorithm of the research methodology.

characteristics of Zr-2.5Nb alloy containing hydrides. Specifically, FEM was used for the determination of the modulus of elasticity and yield strength, P_Q load determination, stress intensity factor calculation, load vs. crack opening displacement curve construction and J-integral calculation.

3. Research object

Zr-2.5Nb TMT-2 alloy used for the manufacture of FC in the Ignalina NPP was chosen as the research object. The non-irradiated section of the fuel channel pipe was provided by Ignalina NPP (Fig. 3). The dimensions of the pipe sample provided were 1.5 m in length, 88 mm in outer diameter and ~ 4 mm in thickness. The sample was divided into 20 segments. Each segment was hydrided at different hydrogen concentration levels. The introduction of hydrogen into the samples was achieved by elevated-temperature electrolytic hydriding (Makarevičius et al., 2001). Subsequent cooling was conducted in a furnace at a rate of 0.5 °C/min, which closely mimics the cooling rate of the fuel channel during reactor shutdown. Such conditions allow for the formation of the zirconium hydrides with the same dimensions that would be found in FC after the shut-down of Ignalina NPP.

4. Numerical determination of mechanical properties of Zr alloy with hydrides

4.1. Measurement of hydride dimensions in zirconium alloy

The concept behind numerically determining the mechanical properties of a zirconium alloy containing hydrides involves simulating a microscale experiment. The assumption is that the behaviour of a single mean-size hydride, which is surrounded by a zirconium alloy matrix and is loaded with uniaxial loading, is aligned with the behaviour of a 37.8 mm long tensile test specimen of a 37.8 mm in length crafted from an FC tube. While the hydrides within the specimen exhibit directional but non-uniform spacing and varying dimensions, these disparities result in distinct effects on material properties at microscale locations within the sample. However, when evaluated at the macro scale, the examination encompasses the entire system. In other words, the experiment provides an average representation of the varying material properties through separate volumes. Consequently, the numerical simulation of a mean-

Fig. 3. Sample of Ignalina NPP fuel channel.

size hydride within a zirconium alloy matrix generates mean values of material properties akin to those observed in the experimental investigation. The microscale model effectively demonstrates how an individual mean-size hydride, without any interaction involving other hydrides, alters the values of mechanical properties of the hydride and zirconium alloy composite system. As such, alignment between the loading direction and hydride orientation in the model and the specimen and the loading direction in the experiment is crucial. Clearly, variations in the dimensions of zirconium hydrides within the alloy lead to differing impacts on the values of the mechanical properties of the zirconium alloy containing hydrides. Therefore, to create the correct model, first, the dimensions of hydrides have to be measured. That was done using the direct measurement technique.

While scrutinising microsection images of the Zr-2.5Nb alloy containing hydrides (Fig. 4), it was observed that varying hydride concentrations within the zirconium alloy led to not only an increased count of hydrides but also variations in their lengths and widths. Also, the orientation across the thickness of the pipe is not uniform. Fig. 5 illustrates the penetration of hydrides through the surface of the FC pipe, occurring perpendicularly to both the inner and outer pipe surfaces However, within the central layers of the pipe, there is a proclivity for hydrides to develop in the axial-tangential (A-T), i.e., axial-circumferential, direction. This inclination toward hydride formation aligns with findings in the pressure tubes of pressurised heavy water reactor designs (Bind et al., 2016). This orientation of zirconium hydrides depends on the crystallographic texture of the FC, which emerges during the processing technology of TMT-2 for RBMK-type reactors.

The measurement of length and width of the hydrides at different hydrogen concentration levels were taken using an OLYMPUS optical microscope directly from the prepared specimens. The results of these measurements are displayed in Fig. 6. However, discerning the extent to which zirconium hydrides occupy the zirconium matrix requires more than just the mean length and width of the hydride. Consequently, an additional evaluation of the hydride volume fraction within the zirconium alloy was conducted using the stereologic planimetric approach (Ohser and Mucklich, 2000). With this methodology, the assumption is made that the area occupied by randomly situated hydrides is consistent across any cross section of the specimen. If this assumption is accepted, the proportionate area taken up by the hydrides may be equalized to the relative volume portion. Microscopic images of the specimen's surfaces were captured using an OLYMPUS optical microscope. The magnifications of the images were 150 and 800 times. The acquired pictures were then post-processed, and hydride volume calculations were carried out using the computer software Scion Image v.4.0.2. An instance of image analysis is depicted in Fig. 7. The image analysis was performed at random positions on the specimen. In addition, to obtain the full picture of the hydrides in two cross-sectional planes were analysed: radial-axial (R-A) and radial-tangential (R-T). No less than 10 analyses were performed in both planes and in each hydrogen concentration. The outcomes of these measurements are summarised in Table 2. The results of the measured hydride area fraction, according to the stereologic planimetric method, represent the volume part of the hydrides within the zirconium matrix.

4.2. FE model of zirconium alloy containing hydride

The concept behind numerically determining the mechanical properties of a zirconium alloy containing hydrides involves simulating an experiment on a microscale. This approach presumes that the behaviour of a mean-sized hydride, which is surrounded by a matrix of zirconium alloy and is loaded by uniaxial load, corresponds to the behaviour observed in a specimen machined from a FC tube and 37.8 mm in length. In the actual experiment, however, the hydrides in the specimen exhibit directional orientation, but lack uniform spacing, and their length, width, and thickness vary. This leads to diverse effects on material properties at distinct volumes within the specimen on microscale. However, when the effects are assessed in macroscale, it encompasses the entire system. In other words, the experiment provides a mean representation of the material's diverse properties across separate microlocations. Consequently, numerical simulation of the tension of the mean-size hydride surrounded by a zirconium alloy gives mean values of the material properties akin to those found in the experiment.

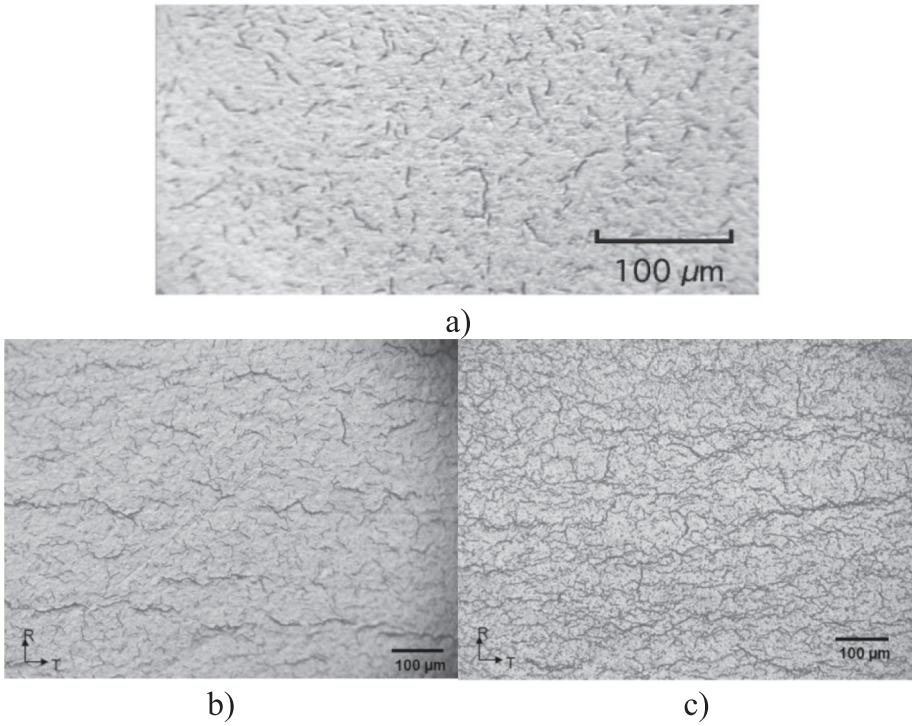

Fig. 4. Picture of the microstructure of the Zr-2.5Nb alloy in the R-T direction at hydrogen concentrations of: a) 45 ppm; b) 100 ppm; c) 250 ppm.

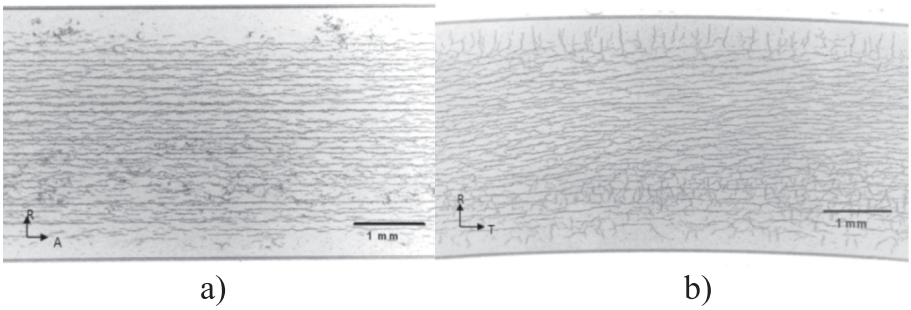

Fig. 5. The view of hydride orientation in the Zr-2.5Nb alloy at 137 ppm hydrogen concentration in: a) R-A direction; b) R-T direction.

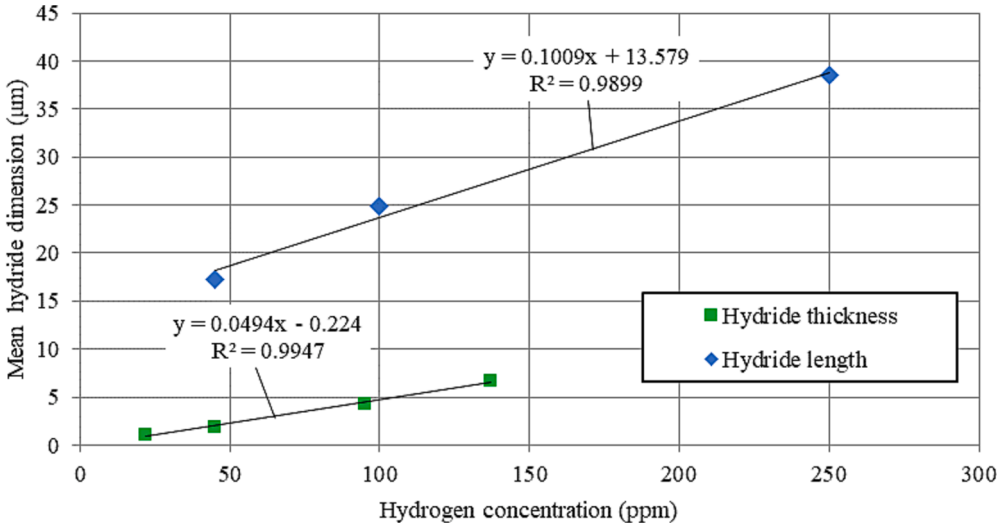

Fig. 6. Zirconium hydride length and thickness in relation to hydrogen concentration.

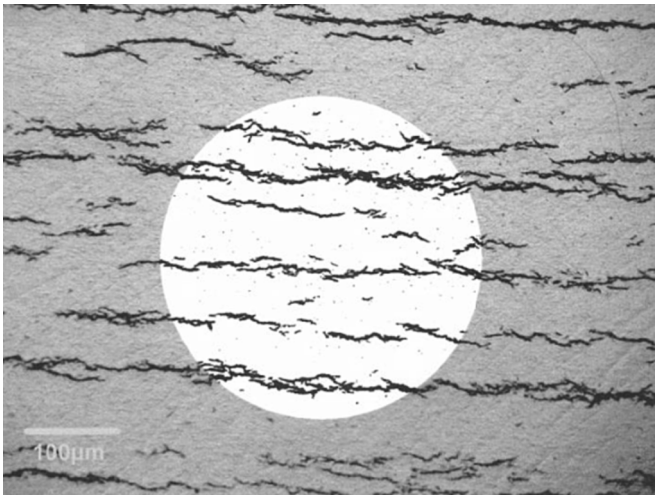

Fig. 7. The view of Scion Image programme for hydride volume fraction measurement at a hydrogen concentration of 137 ppm (measuring surface area 0.17 mm^2).

The microscale numerical model effectively illustrates how a solitary mean-sized hydride induces changes in the mechanical properties of the hydride and zirconium alloy composite system. Therefore, the loading direction and specimen orientation employed in experimental research must match up with the hydride orientation and loading in the numerical simulation.

Table 2
Hydride area fraction measurement results.

Hydrogen concentration (ppm)	Hydride area fraction (%)		
	R-A direction	R-T direction	Mean
23	2.4	3.0	2.7
95	7.4	8.1	7.8
137	10.4	9.1	9.7

A computational model depicting a zirconium alloy matrix with an embedded hydride was generated using ABAQUS finite element (FE) software (ABAQUS/CAE, 2011). The model itself is shown in Fig. 8. As demonstrated in Section 4.1, the hydrides in Zr-2.5Nb alloy of FC are more likely to develop along the axial-tangential direction (Fig. 5). Moreover, in the course of NPP operation, the substantial pressure experienced leads to the highest stress in the tube's circumferential direction, commonly referred to as hoop stress. Consequently, both numerical investigations and experimental studies (Daunys et al., 2008) were conducted in the tube's circumferential (tangential) direction.

The numerical simulation was conducted at varying hydrogen concentrations: 52, 100, and 140 ppm. Consequently, the dimensions of the hydrides within the model differed for each concentration, aligning with the mean measured dimensions of hydrides (Fig. 8). Consequently, the modelled hydride's length ranged from 18.8 to 27.7 μm, while its width ranged from 2.3 to 6.7 μm across the different concentrations. The zirconium matrix that encompasses the hydride was represented in a square shape. The length of the square's edges were chosen in such a way that the area taken by hydride in the model would correlate with the results in Table 2. To mitigate stress concentration, the hydride's end

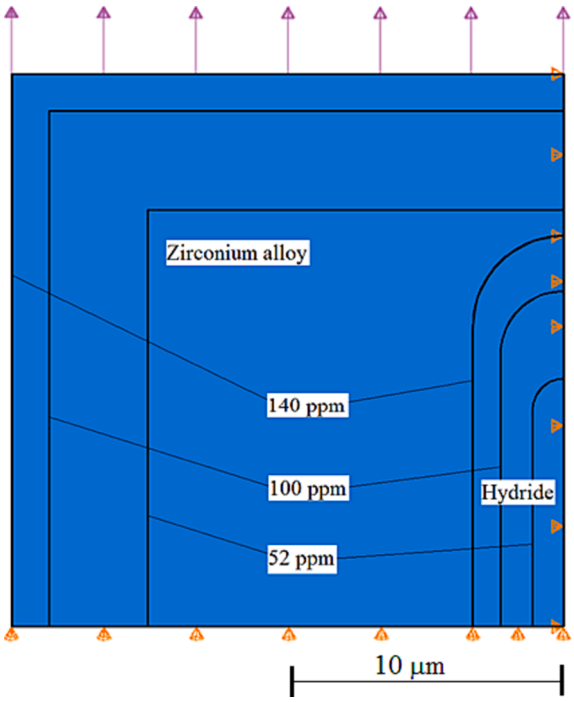

Fig. 8. Micromodel of zirconium alloy with hydride at hydrogen concentrations of 52, 100, and 140 ppm.

was rounded. The radius of the roundness was equal to 1/2 of the thickness of the hydride. To capture symmetry, only one-fourth of the model was generated, considering its dual symmetry planes. The model thickness was set to 1 μm. Symmetry boundary conditions were applied to the bottom edge and vertical edge on the right side of the model (Fig. 8). Displacement served as the load that was added to the upper horizontal edge. After computation, the reaction force was assessed and subsequently transformed into the stresses needed for constructing the stress–strain curve.

The S8R shell elements containing 8 nodes (ABAQUS/CAE, 2011) were used for the mesh. The analysis of mesh size indicated that, due to the simple geometry of the model and the uniaxial nature of the load, the element size does not exert a substantial influence on the calculation results. Hence, 0.5 μm size elements were used to mesh all numerical models.

To describe the behaviour of the zirconium matrix in the model, the mechanical properties shown in Table 3 were used. Here, E – modulus of elasticity, $\sigma_{0.2}$ –relative yield strength, σ_U –ultimate strength, ε_f –failure strain and Z – reduction in the cross-sectional area of the specimen. These properties were sourced from the scientific literature (Daunys et al., 2008). Daunys et al. have experimentally tested the Zr-2.5Nb TMT-2 alloy from Ignalina NPP.

The methodology shown in (Varias and Massih, 2000) was employed to compute the mechanical properties of zirconium hydride. The modulus of elasticity E (Pa) is determined using the following equation:

$$E = (95900 - 57.4 \bullet (T - 273))10^6 \quad (1)$$

here T – temperature, K.

And the ultimate strength is determined by:

$$\sigma_U = 7.35710^{-3}E \quad (2)$$

Table 3
Mechanical properties of Zr alloy.

E (GPa)	σ_U (MPa)	$\sigma_{0.2}$ (MPa)	Z (%)	ε_f (%)
34.4	492	411	62.2	14.78

Having these parameters, the stress–strain curve of the hydride was reconstructed. Fig. 9 shows the true stress–strain curves for both zirconium hydride and the Zr-2.5Nb alloy.

4.3. Numerical evaluation results

The FE models shown in Section 4.2. were used for the determination of stress–strain curves of the zirconium alloy containing hydrides. Calculations were carried out at varying hydrogen concentrations: 52, 100, and 140 ppm. Fig. 10 illustrates the constructed stress–strain curve through numerical modelling at a concentration of 140 ppm. The figure also presents the stress–strain curves of 0 ppm and 140 ppm concentrations, as determined experimentally (Daunys et al., 2008). It is worth noting that the experimental specimens tested in (Daunys et al., 2008) underwent hydriding at the Lithuanian Energy Institute. The conditions for specimen preparation were the same as those for measuring volume fraction and dimensions of hydrides.

The results of the numerical simulation within the elastic range show a satisfactory alignment with the experiment (Fig. 10). However, as the plastic strain initiates, there is a separation between the stresses calculated numerically and those determined by experiment. It is also worth noting that the numerically derived stress–strain curve lacks a stress drop. This means that with increasing strain, the rate of stress growth gradually slows down, but never decreases. Consequently, the absence of stress drop makes the determination of ultimate strength impossible. Fig. 11 presents a comparison between the numerically determined modulus of elasticity and the experimentally determined values (Daunys et al., 2008) over varying hydrogen concentrations. The figure also features the linear regression line based on the experimental data. Both the results from numerical simulation and the experimental findings indicate an upward trend: as the hydrogen concentration rises, the corresponding modulus of elasticity values also increase. This phenomenon can be explained by the fact that an increased hydrogen concentration corresponds to a larger volume fraction of hydrides, thereby amplifying the impact of hydrides on the system's properties.

Table 4 presents a comparison between the numerical modelling results and experimental evaluations of the modulus of elasticity and yield stress of the zirconium alloy containing hydrides. The greatest deviation is up to 9 % between the numerically simulated modulus of elasticity (E) and the experimental values. The deviation in the numerically predicted yield stress, depending on the hydrogen concentration, varies within the range of 11 % to 14 % compared to the experimental results.

As the results show, the numerical simulation results do not deviate from experimental data more than 14 %, therefore, the presented methodology can be used for the evaluation of elastic modulus and yield stress of Zr-2.5Nb alloy containing hydrides. However, the methodology still needs to be improved for higher accuracy.

5. Numerical determination of critical stress intensity factor

5.1. FE model

According to the research algorithm (Fig. 2) the second step is the numerical determination of the critical stress intensity factor K_{IC}. The idea behind the numerical determination of K_{IC} is the simulation of the compact tension experiment according to the ASTM E399-12e3 (2018) standard.

Numerical investigations were conducted at the same hydrogen concentration levels as for the determination of mechanical properties. The analysed material was the same Zr-2.5Nb TMT-2 alloy. The behaviour of the material was characterised using the mechanical properties discussed in Section 4.3. In the current analysis, experimentally determined mechanical properties were used.

The FE model of the C(T) specimen was created, with its dimensions matching those of the actual experimental specimen as described by

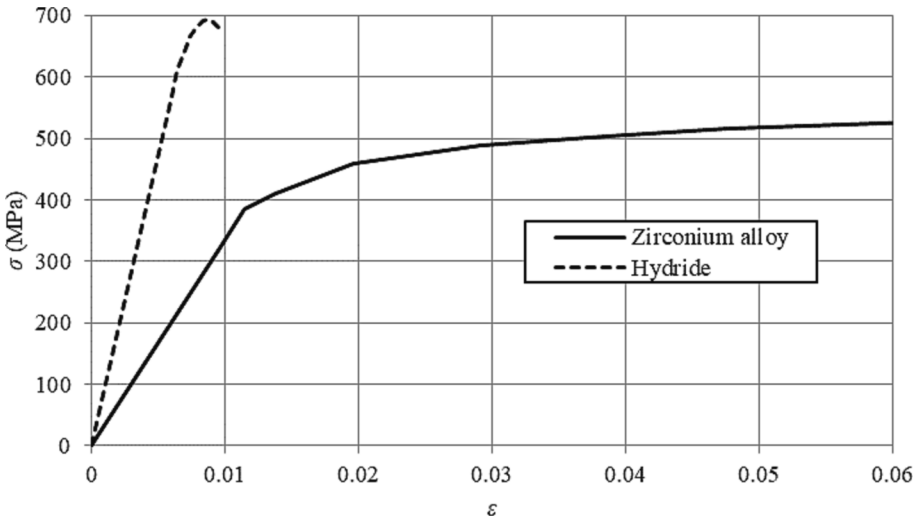

Fig. 9. True stress vs. true strain of the Zr-2.5Nb alloy and zirconium hydride.

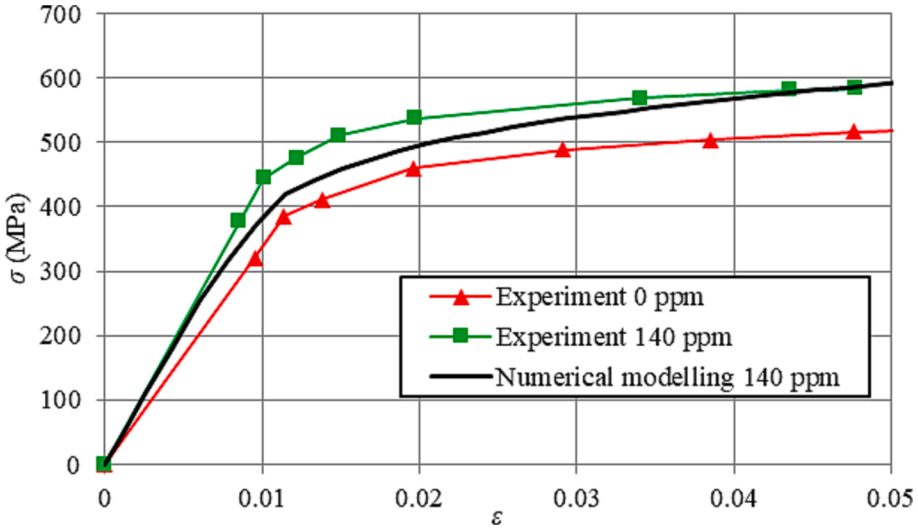

Fig. 10. Stress–strain curves of the Zr-2.5Nb alloy determined both numerically and experimentally.

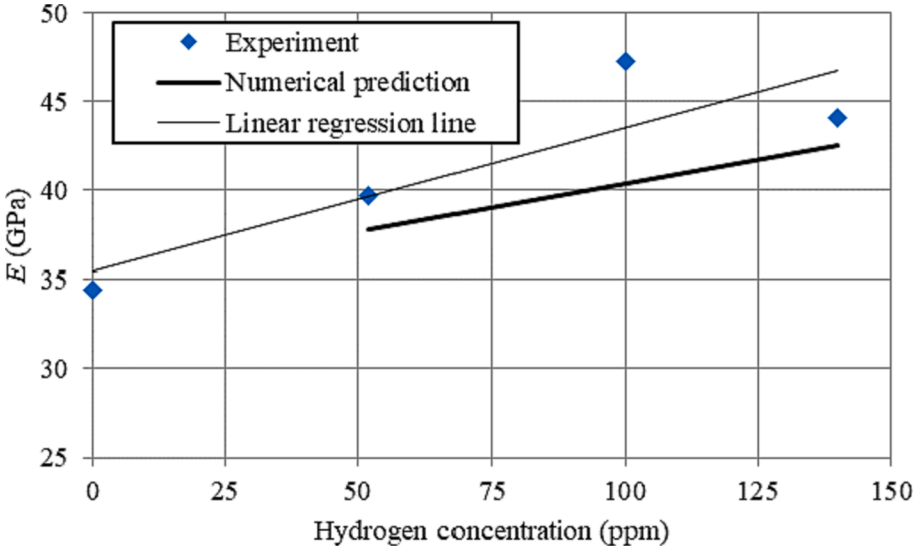

Fig. 11. Modulus of elasticity values determined numerically and experimentally in relation to the hydrogen concentration of the Zr-2.5Nb alloy.

Table 4
The comparison between the results of the numerical simulation and the experimental values of the mechanical properties of the Zr-2.5Nb alloy with hydrides.

Hydrogen concentration (ppm)	E (MPa)		Deviation (%)	$\sigma_{0.2}$ (%)	Deviation (%)		
	Linear regression of the experiment		Numerical modelling		Experiment	Numerical modelling	
52	39.7		37.8	4.8	368	418	13.6
100	43.5		40.4	7.1	470	420	10.6
140	46.7		42.5	9.0	470	420	10.6

Daunys et al. in 2008. The mesh and boundary conditions for the FE model are illustrated in Fig. 12. The difference in this specimen compared with a standard recommended in ASTM E399-12e3 (2018) is the scale. Given that the experimental specimen was constructed from an Ignalina NPP FC tube, with an internal diameter of 79.5 mm and a wall thickness of approximately 4 mm, smaller specimens were tested as recommended in the standard. The dimensions of the experimentally and numerically tested specimen were: width $W = 17$ mm, thickness $B = 4.2$ mm, crack length $a = 6.75$ mm, and fatigue crack length $a_1 = 1.8$ mm. The mesh of the FE model was created using C3D20R elements. The region around the crack underwent meshing through a circular pattern approach, while singular elements were designated at the crack's frontal area. To account for significant displacements and deformations, the nonlinear geometric effect option (Nlgeom) was enabled. Due to the symmetry of the specimen, only one-half of the specimen was modelled, with symmetry boundary conditions applied to the surface highlighted with the grey and red rectangles (refer to Fig. 12). Additional boundary conditions were imposed on the RP point, restricting displacement along the X and Z axes, as well as rotation around the Y axis. The negative displacement of the Y coordinate axis of the RP point was used as a load. Rigid coupling elements connected the RP point to one side of the cylindrical hole (indicated by the yellow surface in Fig. 12). For the measurement of the crack opening displacement, the movement of point P1 was tracked.

5.2. Results of the determination of the critical stress intensity factor

According to ASTM E399-12e3 standard, first the P_Q load should be found at which the so-called conditional stress intensity factor K_Q value is found. And if all the conditions required by the standard are met only then K_Q can be equalised to the critical stress intensity factor K_{IC}., which would be a material fracture parameter otherwise called fracture toughness. To find a P_Q load experimentally, the tension of the C(T) specimen is conducted, where the tension load and crack opening displacement are recorded. Having load vs. crack opening displacement curve P_Q load is found as it is shown in Fig. 13. The P_Q load was computed through nonlinear numerical simulations, during which the elastic–plastic properties of the material were used. P_Q loads were determined for Zr-2.5Nb alloys with thermal treatment TMT-2 at different levels of hydrogen concentration, including cases without hydrogen and with hydrogen concentrations of 52, 100, and 140 ppm. The determined P_Q loads are presented in Fig. 14. The same figure also shows the P_Q loads determined through experimental tests (depicted as diamond-shaped points) according to Daunys et al. (2008), along with their mean values represented by a dotted line. The numerical results show a high level of agreement with the mean values of the experimental data, with a deviation of up to 3 %.

The K_Q values were determined by performing a linear numerical analysis of the C(T) specimen tension where previously found P_Q was used as a loading.

Fig. 15 presents a comparison between the K_Q values obtained through numerical analysis and experimental tests. In the figure, it is evident that all numerically computed K_Q values surpass the average values determined experimentally, although the difference remains within 11 %. Furthermore, the trend in the shape of the numerically calculated K_Q values aligns with the results of the experiment. Specifically, as the hydrogen concentration increases from 0 ppm to 100 ppm, the numerically derived K_Q decreases by 2.99 MPa$\sqrt{\text{m}}$, while the

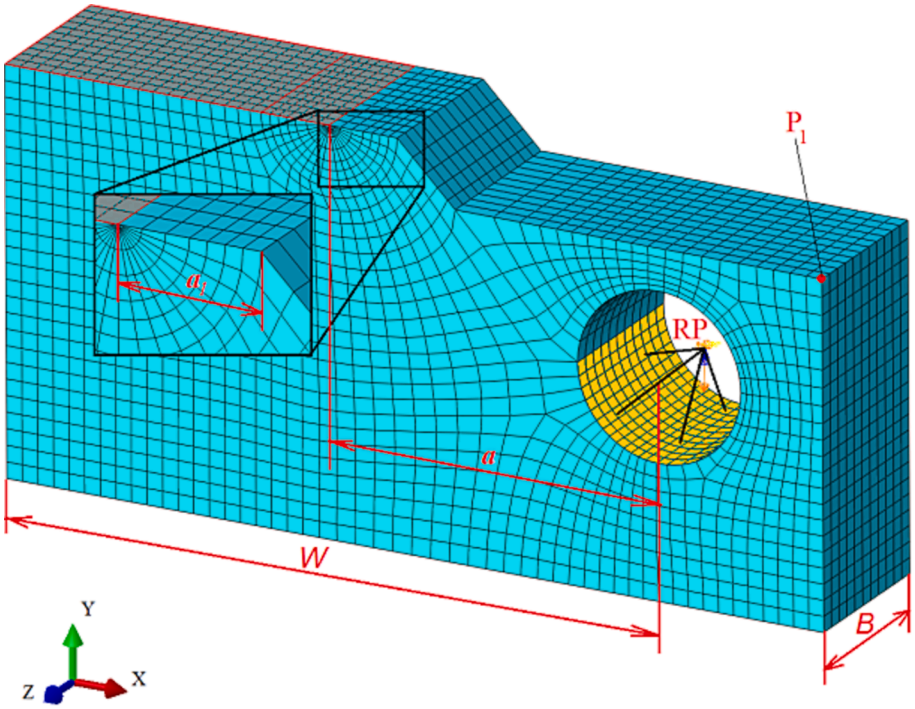

Fig. 12. FE model of C(T) specimen with mesh and boundary conditions.

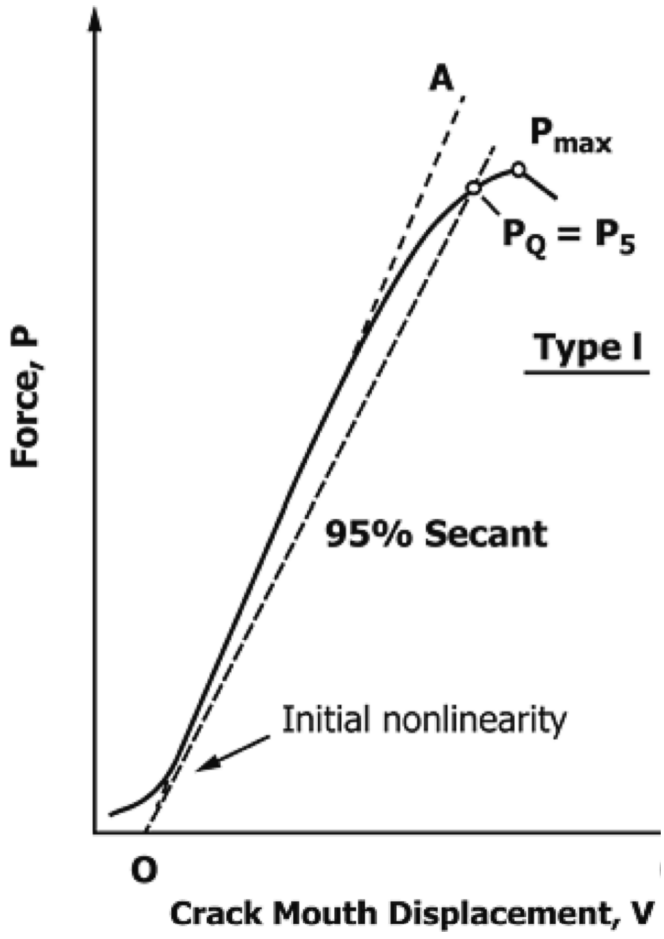

Fig. 13. Force versus crack opening displacement curve for P_Q load determination (ASTM E399-12e3, 2018).

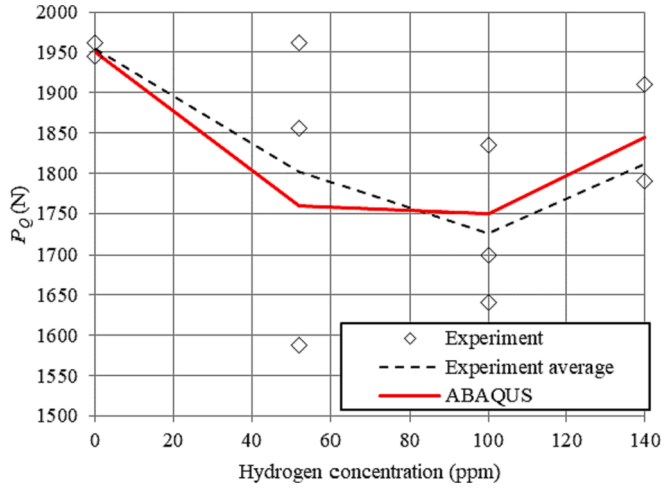

Fig. 14. Comparison of the numerically determined P_Q load with experimental data of the zirconium alloy vs. hydrogen concentration.

experiment value decreases by 4.5 MPa$\sqrt{m}$. This reflects a reduction of 8 % for numerical simulation and 13 % for experiment. Beyond the 100 ppm concentration, there is a slight increase in the K_Q values determined numerically as well as experimentally.

According to ASTM E399-12e3 (2018) requirements, some of the conditions were not satisfied for K_{IC} evaluation. In all calculation cases, the condition $P_{max}/P_Q \leq 1.1$ was not fulfilled (here P_{max} – maximal

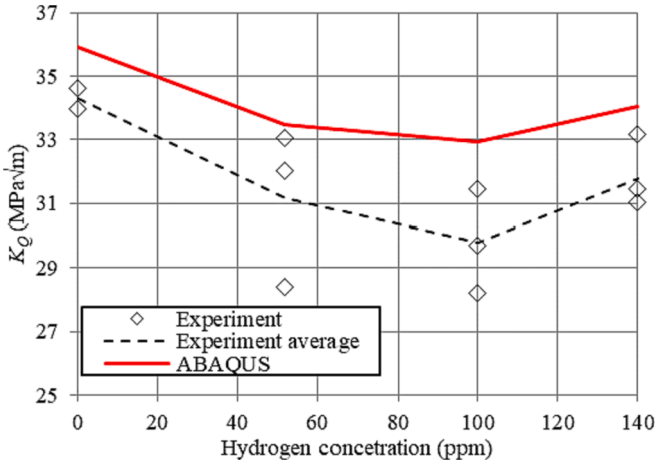

Fig. 15. Comparison of the numerically determined K_Q value with the experimental data factor of the zirconium alloy vs. hydrogen concentration.

tension force, N; see Fig. 13). Therefore, conditional fracture toughness cannot be equalised with the critical stress intensity factor, $K_Q \neq K_{IC}$. This means that even at relatively high hydrogen concentration levels Zr–2.5Nb TMT-2 alloy maintains its ductility and according to the research methodology algorithm (Fig. 2) and the recommendations of the ASTM E399-12e3 (2018) standard, the critical J-integral J_{IC} must be determined.

6. Numerical determination of the critical J-integral

6.1. Methodology for numerical determination

The third step of the research algorithm (Fig. 2) is the numerical determination of the critical J-integral J_{IC} of the zirconium alloy. The main idea behind this research step, the same as for the numerical determination of the K_{IC}, is the simulation of the tension experiment of the C(T) specimen according to ASTM E1820-15a (2015) standard. According to the specifications outlined in this standard for the determination of the critical J-integral J_{IC}, it is necessary to create a curve that depicts the relationship between the J-integral J_I and the extension of the crack Δa. However, numerical simulation of accurate crack extension (growth) is an extremely complicated task. Therefore, in our case, the crack extension was found by solving the second-order polynomial function defined by the ratio between the crack opening displacement V and the load P vs. the crack extension Δa curve. Sullivan and Crooker (1977) introduced an approach in which crack opening displacements were used to find the crack extension. They proposed the utilisation of a polynomial function $a/W = f(E,B,V,P)$ for this purpose. Given that this polynomial function will be integrated into the developed methodology to numerically determine the fracture toughness for assessing the extension of the crack, we suggest substituting the length of the crack a with the crack extension Δa. In this research step, mechanical properties were used the same as in the K_{IC} calculation for nonlinear analysis. Determined J_{IC} results were compared with the experimental data found in (Daunys et al., 2008).

For the numerical calculation of J_{IC}, the identical FE model employed in the determination of K_{IC} (as detailed in Section 5.1 and depicted in Fig. 12) was utilised. Only the fatigue crack length a_1 was slightly longer and equal to 2.2 mm. In addition, the point for measuring the crack opening displacement was changed to the RP point. The results of numerical simulations for the C(T) specimen tension tests are illustrated in Fig. 16. The numerical calculation results are compared with the values obtained by experimental tests. It is evident that, at lower levels of crack mouth opening V, a strong alignment between numerical and experimental findings was observed across all cases. However, in the case of

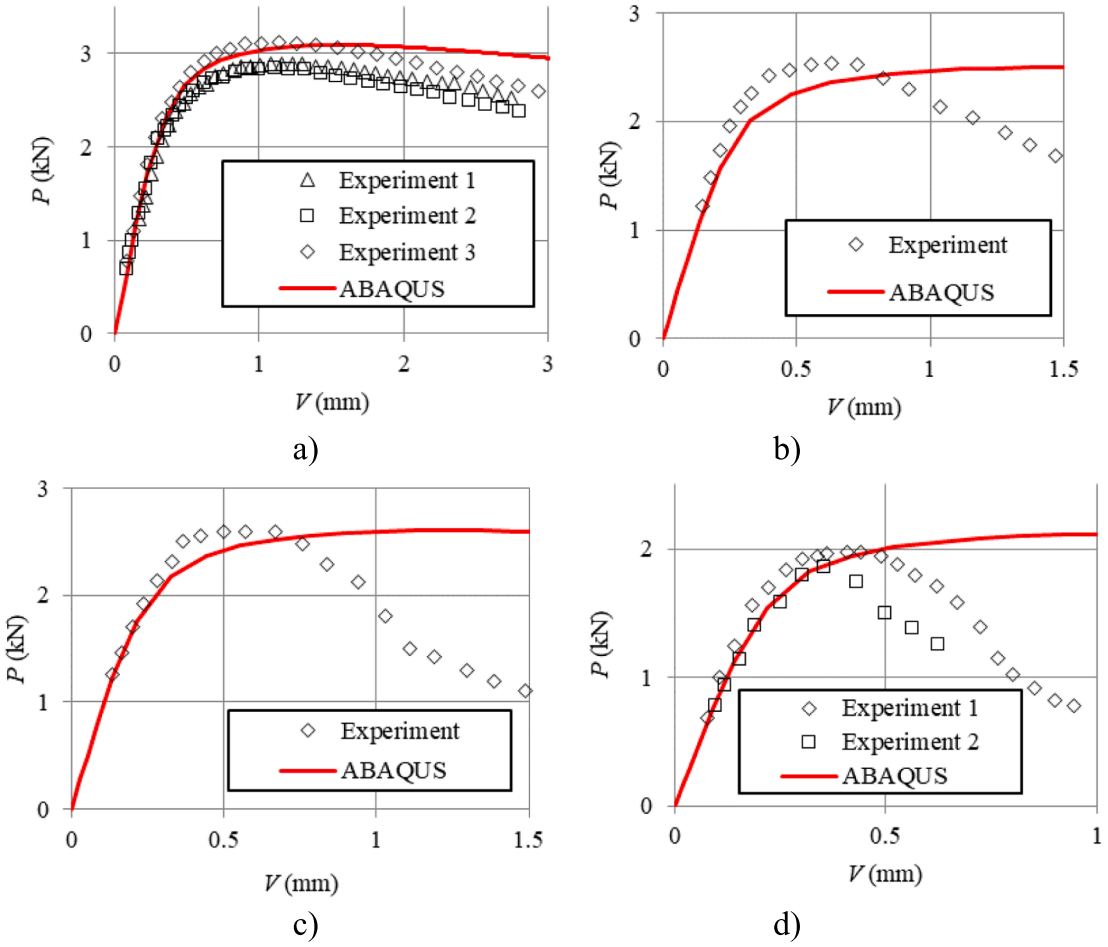

Fig. 16. Comparison of numerically determined *P-V* curves with experimental data at hydrogen concentrations: a) 0 ppm; b) 52 ppm; c) 100 ppm; d) 140 ppm.

zirconium alloys containing hydrides, the deviation between numerical and experimental results emerges as the *V* values exceed the peaks of the experimental curves. Despite this disparity, the tensile forces P_{max} determined by numerical simulation remain in close proximity to the experimental values, with deviations not exceeding 5 %.

6.2. Results of the numerical determination of critical J-integral

To find the polynomial function, experimental data from studies on the Zr-2.5Nb TMT-2 alloy without hydrogen, as conducted by Daunys et al. in 2008, were used. The established relationships between *EBV/P* on $\Delta a/W$ are shown in Fig. 17. The second-order polynomial equation derived from the mean curve is as follows:

$$\frac{EBV}{P} = 15719\left(\frac{\Delta a}{W}\right)^2 + 2401.5\left(\frac{\Delta a}{W}\right) + 45.155. \quad (3)$$

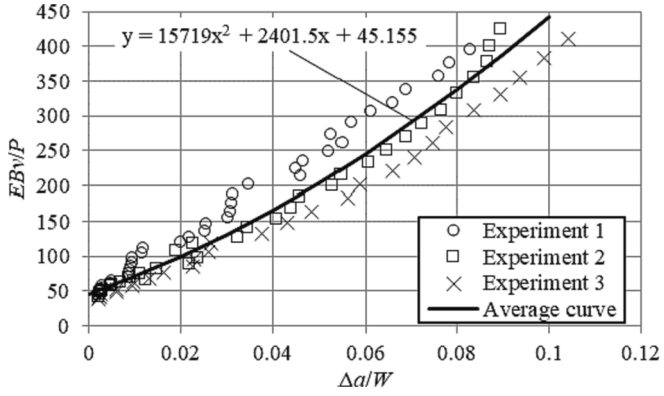

Fig. 17. *Dependence of* EBv/P_{max} on $\Delta a/W$ of zirconium alloy without hydrogen.

To determine J_Q, the J_I-Δa curves were generated using Equation (3) along with the results of the numerical simulation. An illustration of a numerically derived J_I-Δa curve for zirconium alloy without hydrogen is displayed in Fig. 18. In particular, the curve derived from the numerical simulation lies within the range of the experimental data until $\Delta a = 1.2$ mm, which indicates good alignment with the experiment. As indicated in the ASTM E1820-15a (2015) standard, first the conditional J-integral value J_Q should be found and if all conditions required by the standard are met only then J_Q can be equalised to elastic fracture toughness J_{IC}. J_Q can be found at the intersection point of J_I-Δa curve and an offset line of 0.2 mm. And, as shown in the figure, in the case of Zr alloy without hydrogen, the conditional J-integral value $J_Q = 104$ kN/m.

ASTM E1820-15a (2015) standard requirements and conditions have been checked for all simulations and all have been met. Hence, it is possible to conclude that the derived value of J_Q is equal to J_{IC} for all cases, whether with or without hydrides. In other words, it can be stated that fracture toughness has been found for the Zr-2.5Nb alloy with and without hydride.

Comparison of numerically evaluated J_{IC} with experimental data is shown as the dependencies of J_{IC} on hydrogen concentration (Fig. 19). The J_{IC} values obtained numerically show a reduction of 68 %, that is, from 104 kN/m to 33 kN/m, while the experimental values show a more substantial decrease of 84 %, that is, from 95 kN/m to 15 kN/m, as the hydrogen concentration rises from 0 ppm to 140 ppm. A good

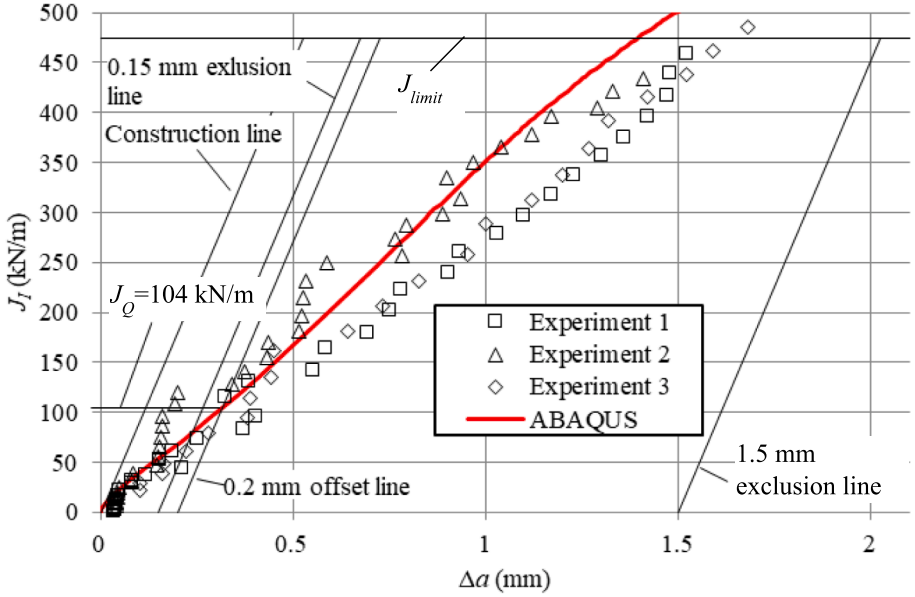

Fig. 18. Comparison of the numerically determined J_I-Δa curve with the experimental data for the zirconium alloy without hydrogen.

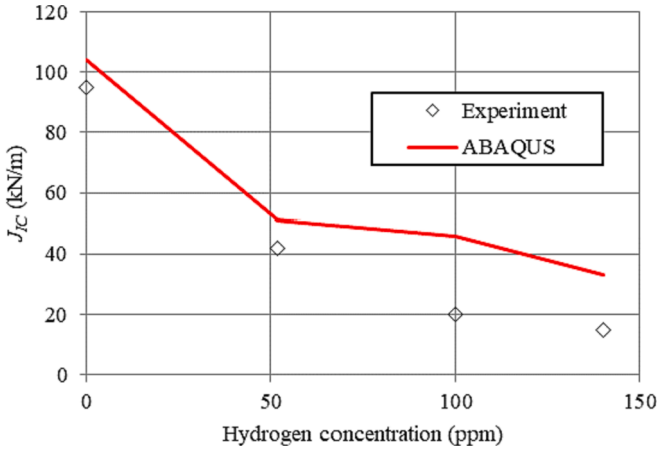

Fig. 19. Comparison of numerically determined J_{IC} values with experimental data vs. hydrogen concentration.

correlation between the numerical and experimental results is evident up to a concentration of 52 ppm. The deviation of numerical simulation results from experimental values deviates up to 20 % when the hydrogen concentration remains under 52 ppm. However, beyond this threshold, the deviation between the numerical and experimental results increases as the hydrogen concentration continues to rise.

On the basis of the acquired results, it is recommended to use the developed numerical methodology along with the derived polynomial function (Eq. (3) to estimate the fracture toughness of the Zr-2.5Nb TMT-2 alloy within the hydrogen concentration limit of up to 52 ppm. This particular threshold proves sufficient for fracture characterisation, considering that RBMK-type reactors tend to maintain an average hydrogen concentration of 52 ppm after 30 years of operation (IAEA, 1996). For estimating fracture toughness beyond the 52 ppm hydrogen concentration, it becomes necessary to improve the precision of numerical evaluation. Achieving this can involve conducting an expanded series of experimental tests on a zirconium alloy, which, in turn, results in a more accurate determination of the polynomial function for crack extension assessment.

7. Conclusions

This paper presents the application of a methodology for numerical investigation of the fracture toughness of zirconium alloy containing hydrides, resulting in the following conclusions:

1. The methodology developed to determine the mechanical properties of zirconium alloy containing hydrides, when compared with the results of the experiment, yields a modulus of elasticity with a deviation of 9 % and a yield strength with a deviation of 14 %.
2. Numerically determined P_Q values compared to experimental data show deviations of only up to 5 %. Similarly, the numerically obtained K_Q values deviate no more than 10 % from the experimental data. This shows the suitability of the numerical approach presented for assessing the elastic fracture toughness. However, the study also highlights that the Zr-2.5Nb TMT-2 alloy retains its ductility even at a relatively high hydrogen concentration, that is, 140 ppm, requiring the determination of elastic–plastic fracture toughness.
3. By employing the second-order derived polynomial equation, it allows predicting crack growth within the C(T) specimen. In particular, the simulated crack growth is 10 % higher than the corresponding experimental results.
4. The numerically determined J_{IC} for Zr alloy containing hydrides surpass the experimentally obtained values by up to 20 % when the hydrogen concentration remains under 52 ppm. With increasing hydrogen concentration, the deviation in numerical determination also rises. Since the numerical and experimental results agree relatively well, it is advised to employ the presented methodology and the polynomial equation to evaluate the fracture toughness of the Zr-2.5Nb alloy with thermomechanical treatment TMT-2 up to the 52 ppm hydrogen concentration threshold.

CRediT authorship contribution statement

Remigijus Janulionis: Methodology, Software, Validation, Formal analysis, Writing – original draft. **Gintautas Dundulis:** Conceptualization, Methodology, Validation, Writing – review & editing.

Declaration of competing interest

The authors declare that they have no known competing financial

interests or personal relationships that could have appeared to influence the work reported in this paper.

Data availability

Data will be made available on request.

References

ABAQUS/CAE, 2011. User's Manual, Version 6.11.

Almenas, K., Kaliatka, A., Ušpuras, E., 1998. Ignalina rbmk-1500. A source book, Extended and updated version. Lithuania. ISBN 9986-492-35-1.

Alvarez Holston, A.M., Stjärnsäter, J., 2017. On the effect of temperature on the threshold stress intensity factor of delayed hydride cracking in light water reactor fuel cladding. Nucl. Eng. Technol. 49 (4), 663–667. https://doi.org/10.1016/j.net.2017.04.002.

ASTM E1820-15a, 2015. Standard Test Method for Measurement of Fracture Toughness.

ASTM E399-12e3, 2018. Standard Test Method for Linear-Elastic Plane-Strain Fracture Toughness KIc of Metallic Materials.

Bind, A.K., Sunil, S., Singh, R.N., 2016. Effect of hydrogen isotope content on tensile flow behavior of Zr-2.5Nb pressure tube material between 25 and 300 °c. J. Nucl. Mater. 476, 5–12. https://doi.org/10.1016/j.jnucmat.2016.04.019.

Bind, A.K., Singh, R.N., Sunil, S., Chattopadhyay, J., 2017. Effect of deuterium content on fracture toughness of Zr-2.5Nb pressure tube material in the temperature range of ambient to 300 C. J. Nucl. Mater. 496, 182–192. https://doi.org/10.1016/j.jnucmat.2017.08.040.

Chakraborty, P., Moitra, A., Saha-Dasgupta, T., 2015. Effect of hydrogen on degradation mechanism of zirconium: A molecular dynamics study. J. Nucl. Mater. 466, 172–178. https://doi.org/10.1016/j.jnucmat.2015.07.031.

Cheadle, B.A., Coleman, C.E., Rodgers, D.K., Davies, P.H., Chow, C.K., Griffiths, M., 1987. Examination of core components removed from CANDU reactors. Proceedings of The Canadian Nuclear Society CANDU maintenance conference. 22-24 Nov., Toronto, Canada.

Cheadle, B.A., Celovsky, A., Ghafoor, M., Butt, W., Brunswick, N., 1996. Assesment of the Integrity of KANUPP Fuel Channels. Proceedings of the seventeenth annual Canadian Nuclear Society conference. Fredericton, New Brunswick, Canada.

Daunys, M., Dundulis, R., Grybėnas, A., Krasauskas, P., 2008. Hydrogen influence on mechanical and fracture mechanics characteristics of zirconium Zr–2.5Nb alloy at ambient and elevated temperatures. Nucl. Eng. Des. 238 (10), 2536–2545. https://doi.org/10.1016/j.nucengdes.2008.05.018.

Grigoriev, V., Josefsson, B., 1998. On the mechanism of Zircaloy cladding axial splits. J. Nucl. Mater. 257 (2), 99–107. https://doi.org/10.1016/S0022-3115(98)00445-0.

Hong, J.D., Kim, H.C., Kim, J.S., Yang, Y.S., Kook, D.H., 2017. Delayed hydride cracking assessment of PWR spent fuel during dry storage. Nucl. Eng. Des. 322, 324–330. https://doi.org/10.1016/j.nucengdes.2017.07.015.

Hsu, H.H., 2006. An evaluation of hydrided Zircaloy-4 cladding fracture behavior by X-specimen test. J. Alloy. Compd. 426 (1–2), 256–262. https://doi.org/10.1016/j.jallcom.2005.12.113.

Iaea, 1999. RBMK fuel channel integrity. A Publication of the Extrabudgetary Programme on the Safety of WWER and RBMK Nuclear Power Plants. Viena, Austria. ISSN 1025–2754.

IAEA, 1996. Water channel reactor fuels and fuel channels: Design, performance, research and development. IAEA - TECDOC-997. Vienna, Austria.

IAEA, 2004. Delayed Hydride Cracking in Zirconium Alloys in Pressure Tube Nuclear Reactors. IAEA-TECDOC-1410. Vienna, Austria.

IAEA, 2006. Understanding and managing ageing of material in spent fuel storage facilities. IAEA Technical Report No. 443, Vienna, Austria.

Ishizuka, N., Nakai, K., Takayama, K., 2003. The pressure tube inspection and integrity evaluation in Fugen. Proceedings of International conference on global environment and advanced nuclear power plants (GENES4/ANP2003). Tokyo Institute of Technology, Tokyo, Japan. 15–19.

Ivanova, S.V., 2002. Effect of hydrogen on serviceability of zirconium items in VVER and RBMK-type reactors fuel assemblies. Int. J. Hydrogen Energy 27 (7–8), 819–824. https://doi.org/10.1016/S0360-3199(01)00160-4.

Jang, K.N., Kim, K.T., 2017. The effect of neutron irradiation on hydride reorientation and mechanical property degradation of zirconium alloy cladding. Nucl. Eng. Technol. 49 (7), 1472–1482. https://doi.org/10.1016/j.net.2017.05.006.

Jeon, J.Y., Kim, Y.J., Lee, S.Y., Kim, J.W., 2016. Extracting ductile fracture toughness from small punch test data using numerical modeling. Int. J. Press. Vessel. Pip. 139–140, 204–219. https://doi.org/10.1016/j.ijpvp.2016.02.011.

Kearns, J.J., 1967. Terminal solubility and partitioning of hydrogen in the alpha phase of zirconium, Zircaloy-2 and Zircaloy-4. J. Nucl. Mater. 22 (3), 292–303. https://doi.org/10.1016/0022-3115(67)90047-5.

Kim, Y.S., 2008. Delayed hydride cracking of spent fuel rods in dry storage. J. Nucl. Mater. 378 (1), 30–34. https://doi.org/10.1016/j.jnucmat.2008.04.011.

Kim, J.H., Lee, M.H., Choi, B.K., Jeong, Y.H., 2007. Effect of the hydrogen contents on the circumferential mechanical properties of zirconium alloy claddings. J. Alloy. Compd. 431 (1–2), 155–161. https://doi.org/10.1016/j.jallcom.2006.05.074.

Kreyns, P.H., Bourgeois, W.F., White, C.J., Charpentier, P.L., Kammenzind, B.F., Franklin, D.G., 1996. Embrittlement of Reactor Core Materials. Proceedings of the Zirconium in the Nuclear Industry: Eleventh International Symposium. 100 Barr Harbor Drive, PO Box C700, West Conshohocken, PA 19428-2959 : ASTM International. 758–782. 10.1520/STP16200S.

Lin, S.C., Hamasaki, M., Chuang, Y.D., 1979. The Effect of Dispersion and Spheroidization Treatment of δ Zirconium Hydrides on the Mechanical Properties of Zircaloy. Nucl. Sci. Eng. 71 (3), 251–266. https://doi.org/10.13182/NSE79-A19062.

Mahler, M., Aktaa, J., 2014. Approach for Determining Fracture Mechanical Properties from Tests on Small Size Specimens at Room Temperature. Procedia Mater. Sci. 3, 434–439. https://doi.org/10.1016/j.mspro.2014.06.073.

Mahler, M., Aktaa, J., 2016. Prediction of fracture toughness based on experiments with sub-size specimens in the brittle and ductile regimes. J. Nucl. Mater. 472, 178–185. https://doi.org/10.1016/j.jnucmat.2015.08.046.

Makarevičius, V., Grybėnas, A., Levinskas, R., 2001. Controlled hydriding of Zr-2.5%Nb alloy by thermal diffusion. Mater. Sci. 7 (4), 249–251.

Motta, A.T., Capolungo, L., Chen, L.Q., Cinbiz, M.N., Daymond, M.R., Koss, D.A., Lacroix, E., Pastore, G., Simon, P.C.A., Tonks, M.R., Wirth, B.D., Zikry, M.A., 2019. Hydrogen in zirconium alloys: A review. J. Nucl. Mater. 518, 440–460. https://doi.org/10.1016/j.jnucmat.2019.02.042.

Ohser J., Mucklich F., 2000. Statistical Analysis of Microstructures in Material Science. John Wiley & Sons, Ltd, 381 p. ISBN 978-0-471-97486-4.

Platonov, P.A., Ryazantseva, A.V., Saenko, G.P., Knizhnikov, Y.N., Viktorov, V.F., 1988. The study of the cause of cracking in zirconium alloy fuel channel tubes. Proceedings of the ASTM Zirconium in the Nuclear Industry - 8th International Symposium.

Silva, C., Leonard, K., Trammel, M., Bryan, C., 2018. Characterization of different forms of Zr-2.5Nb samples before and after neutron irradiation. Mater. Sci. Eng. A 716, 296–307. https://doi.org/10.1016/j.msea.2018.01.059.

Simpson, L.A., Cann, C.D., 1979. Fracture toughness of zirconium hydride and its influence on the crack resistance of zirconium alloys. J. Nucl. Mater. 87 (2–3), 303–316. https://doi.org/10.1016/0022-3115(79)90567-1.

Sullivan, A.M., Crooker, T.W., 1977. A crack-opening-displacement technique for crack length measurement in fatigue crack growth rate testing—development and evaluation. Eng. Fract. Mech. 9 (1), 159–166. https://doi.org/10.1016/0013-7944(77)90061-3.

Suman, S., Khan, M.K., Pathak, M., Singh, R.N., Chakravartty, J.K., 2015. Hydrogen in Zircaloy: Mechanism and its impacts. Int. J. Hydrogen Energy 40 (17), 5976–5994. https://doi.org/10.1016/j.ijhydene.2015.03.049.

Suman, S., Khan, M.K., Pathak, M., Singh, R.N., 2017. Effects of Hydride on Crack Propagation in Zircaloy-4. Procedia Eng. 173, 1185–1190. https://doi.org/10.1016/j.proeng.2016.12.105.

Varias, A.G., Massih, A.R., 2000. Temperature and constraint effects on hydride fracture in zirconium alloys. Eng. Fract. Mech. 65 (1), 29–54. https://doi.org/10.1016/S0013-7944(99)00107-1.

Videm, K., Lunde, L., Hollowell, T., Vilpponen, K., Vitanza, C., 1979. Cracking of cladding tubes caused by power ramping and by laboratory stress corrosion experiments. J. Nucl. Mater. 87 (2–3), 259–267. https://doi.org/10.1016/0022-3115(79)90562-2.

Weygand, S.M., Aktaa, J., 2009. A numerical study of the size effect in fracture mechanical bending tests with the cohesive zone method. J. Nucl. Mater. 386–388, 971–973. https://doi.org/10.1016/j.jnucmat.2008.12.264.

Yeniscavich, W., Wolfe, R.A., Lieberman, R.M., 1959. Hydrogen absorption by nickel enriched zircaloy-2. J. Nucl. Mater. 1 (3), 271–280. https://doi.org/10.1016/0022-3115(59)90023-6.